Long-cavity all-fiber ring laser actively mode locked with an in-fiber bandpass acousto-optic modulator

C. Cuadrado-Laborde,[1,2,3,*] M. Bello-Jiménez,[1,4] A. Díez,[1] J. L. Cruz,[1] and M. V. Andrés[1]

[1]*Departamento de Física Aplicada, ICMUV, Universidad de Valencia, Dr. Moliner 50, Burjassot E-46100, Spain*

[2]*CIOp (CONICET La Plata-CIC), P.O. Box 3, Gonnet 1897, Buenos Aires, Argentina*

[3]*Facultad de Ciencias Exactas e Ingeniería, Universidad Católica de La Plata, Buenos Aires, Argentina*

[4]*Instituto de Investigación en Comunicación Óptica (IICO), Universidad Autónoma de San Luis Potosí, Av. Karakorum 1470, Lomas 4a Secc., 78210 San Luis Potosí, S.L.P., Mexico*

**Corresponding author: Christian.Cuadrado@uv.es*

Received October 17, 2013; revised November 16, 2013; accepted November 18, 2013; posted November 22, 2013 (Doc. ID 199674); published December 19, 2013

We demonstrate low-frequency active mode locking of an erbium-doped all-fiber ring laser. As the mode locker, we used a new in-fiber bandpass acousto-optic modulator showing 74% modulation depth, 3.7 dB power insertion losses, 4.5 nm of optical bandwidth, and 20 dB of nonresonant light suppression. The laser generates 330 ps mode-locked pulses over a 10 ns pedestal, at a 1.538 MHz frequency, with 130 mW of pump power.

OCIS codes: (140.4050) Mode-locked lasers; (140.3510) Lasers, fiber; (140.3500) Lasers, erbium; (230.1040) Acousto-optical devices.

http://dx.doi.org/10.1364/OL.39.000068

Many applications encompassing micromachining, biomedicine, optical measurement instruments, and high-resolution ranging (lidar) systems, among others, demand few megahertz frequency, subnanosecond pulse width fiber laser systems. Low-repetition-rate femtosecond or picosecond lasers could serve as a seed source for a chirped pulse amplification system to generate high-energy pulses. These requirements preclude the use of standard *Q*-switched lasers. In mode-locked lasers, output light pulses have subnanoseconds pulse widths but repetition rates generally above the tens-of-megahertz regime. One solution employed in this case is to use pulse pickers. However, the reduction of the repetition rate with this method introduces energy losses and backreflection, impairs the signal-to-noise ratio, and increases complexity. For this reason, very recently, low-frequency mode-locked lasers have been proposed as an alternative to overcome these difficulties [1–4]. For mode-locked lasers, lower repetition rates require longer laser cavities; however, for fiber cavities this is not a major issue, since the fiber may be easily spooled. It is also worth mentioning that all these proposals were based on passive mode-locking techniques. However, when subnanosecond pulses at about 1 MHz repetition rate are required, it is worthwhile to investigate the possibility of using active mode locking. There are applications in which an active mode-locking scheme is preferred, e.g., for applications needing synchronization to a master clock or when several lasers sources or instruments must be operated synchronously, and, in addition, active mode locking prevents start and multiple peak problems that passive approaches may present. One element that is key in the development of an actively mode-locked strictly all-fiber laser is the modulator [5]. The use of in-fiber modulators is an attractive solution, because there will be potentially low losses and it prevents etalon formation, which can frustrate the mode locking, and provides a robust all-fiber cavity [6,7].

In an optical fiber, the fundamental mode guided by the core and the modes supported by the cladding can be coupled by a periodic perturbation [8]. The optical coupling takes place at the optical wavelength that verifies the phase-matching condition between the optical modes and the periodicity of the perturbation. The acousto-optic modulator (AOM) proposed in this work could be seen as an acoustically induced long-period grating (AI-LPG) with a core mode blocker (CMB) in the middle. Figure 1(a) depicts the operation principle by coupling the LP_{01} core mode to a cladding mode. Thus, the core mode LP_{01} is first coupled to a cladding mode by the first part of the AI-LPG and bypasses the CMB via cladding propagation, later being coupled back to the core mode LP_{01} by the second part of the AI-LPG. The device works as a bandpass filter, and thus light whose wavelength does not verify the phase-matching condition

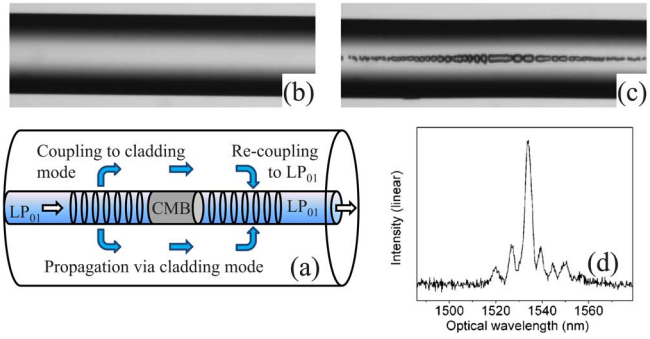

Fig. 1. (a) Schematic of the AOM operation principle. Optical fiber (b) before and (c) after the electrical arch discharges. (d) Spectrum in transmission of the AOM when the piezoelectric is excited with a sinusoidal signal at 769 kHz and 40 V.

is strongly attenuated by the CMB. By using traveling flexural acoustic waves, this device behaves as an all-fiber acousto-optic bandpass filter whose spectral characteristics remain fixed as long as the acoustic signal does not change [9]. In this work, however, we demonstrate the possibility of using this device as an all-fiber acousto-optic amplitude modulator in the megahertz range, by using standing, instead of traveling, flexural acoustic waves. Recently, we proposed a new in-fiber AOM consisting of a single AI-LPG [6], which behaves essentially as a band-stop filter; for this reason, an additional filter was also necessary within the cavity for mode-locking operation. However, in our new proposal no additional filtering devices are necessary due to the modulator's bandpass characteristics. This greatly simplifies the design and operation of the mode-locked laser, since no spectral tuning is necessary between different optical components within the cavity.

The CMB was made by locally heating a previously H_2-loaded B–Ge codoped fiber for 90 days at 15 bars (Fibercore PS1250/1500). When the H_2-loaded B–Ge codoped fiber is exposed to successive electric arc discharges in a fusion splicer, it leads to microexplosions within the core [10]. Thus, the core of the fiber is destroyed such that light is no longer guided by the fundamental mode. In this specific case, three arc discharges of 10 mA and 300 ms each were enough to induce a 20 dB attenuation in the core mode. Figures 1(b) and 1(c) show a detailed photograph of the optical fiber before and after the electrical arc discharges, respectively. The affected core region, which operates like the CMB, can be easily observed in Fig. 1(c); special attention should be paid here to the fact that the cladding was unaffected by the microexplosions. This is essential for avoiding substantial acoustic reflections, which would lessen the coupling back to the core mode of the light propagating by the cladding in the second part of the AI-LPG. Finally, in order to enhance the acousto-optic interaction, the fiber was chemically etched in a hydrofluoric acid bath. The final dimensions of the tapered fiber were 0.4 m and 63 μm for the taper length and waist diameter, respectively. The CMB was located nearly in the middle of the tapered fiber. The AOM is completed by the radio-frequency (RF) source, a piezoelectric, an aluminum conical horn, and a holder. The horn is attached to the piezoelectric, and it focuses the vibrations into the tapered fiber through its tip, which is glued close to the transition of the tapered fiber, approximately at 0.3 m of the CMB.

The transmission properties of the AOM were investigated by illuminating the device with a broadband light source and detecting the transmitted light with an optical spectrum analyzer. Figure 1(d) shows the spectrum when a flexural acoustic wave at 769 kHz travels down the AOM for an applied voltage to the piezoelectric of 40 V (whenever we refer to voltages, it is a peak-to-peak measurement). The transmission peak is located at 1534.45 nm, with a measured FWHM of 3.2 nm. At this wavelength the coupling between the core mode LP_{01} and the cladding mode produces the maximum transfer of energy. The period of the AI-LPG is estimated to be 854 μm, obtained from the dispersion relation for a flexural acoustic wave on a cylindrical rod $\Lambda = \sqrt{(\pi w C_f/2\nu_a)}$, where Λ is the acoustic wavelength, w is the taper waist

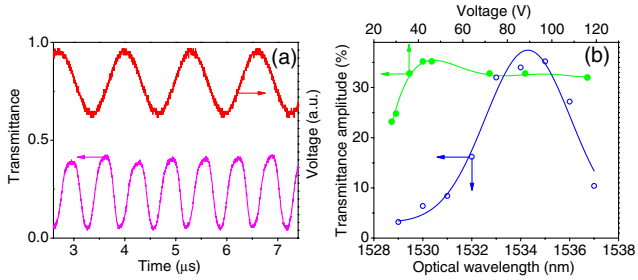

Fig. 2. (a) Optical signal transmitted by the AOM (purple curve, left axis), together with an RF signal of 40 V and 769 kHz applied to the piezoelectric (red curve, right axis). (b) Transmittance amplitude as a function of the applied voltage for a fixed acoustic frequency of 769 kHz and optical wavelength of 1534.45 nm (solid green scatter points, top axis) and transmittance amplitude as a function of the optical wavelength for a fixed acoustic frequency of 769 kHz and applied voltage of 40 V (open blue scatter points, lower axis).

diameter, C_f is the speed of the extensional wave (5760 ms^{-1} for fused silica), and ν_a is the acoustic wave frequency (769 kHz). This acousto-optic interaction produces no amplitude modulation on the transmitted signal. However, by clamping the end of the tapered fiber opposite to the silica horn, a standing acoustic wave can be generated. In this case, the transmitted light rises and falls at twice the frequency of the electrical signal, i.e., a modulation frequency $f_m = 2 \times 769$ kHz = 1.538 MHz. Figure 2(a) shows the optical signal transmitted by the AOM when a standing acoustic wave is applied, together with the voltage of the RF signal applied to the piezoelectric. The measurement was performed by tuning a laser diode to the maximum of the transmittance, i.e., 1534.45 nm [see Fig. 1(d)], and measuring the transmitted light, for a fixed frequency of the RF signal of 769 kHz. The minimum transmittance is 0.06 (−12 dB), which differs from the attenuation of 20 dB produced by the CMB when no acoustic signal is launched to the AOM. This is because the AI-LPG does not strictly vanish periodically (as it should in the case of a pure standing acoustic wave), due to a nonunitary acoustic reflectivity at the end of the acoustic resonator. Figure 2(b) shows the transmittance amplitude—defined as the difference between the maximum and minimum transmittance—as a function of the applied voltage. This AOM shows a transmittance amplitude of 35% for an applied voltage of 42 V. The corresponding modulation depth—defined as $(I_{max} - I_{min})/(I_{max} + I_{min})$, where I_{max} and I_{min} are the maximum and minimum transmitted intensities, respectively—is 74%. Finally, the insertion loss—determined from the maximum transmittance—was 3.7 dB. Beyond this voltage the intensity of the transmission peak reduces gradually, due to the periodic dependence of mode coupling on the intensity of the acoustic signal. We also measured the dependence of the transmittance amplitude on the optical wavelength, by fixing both the acoustic frequency and the applied voltage to the piezoelectric: 769 kHz and 40 V, respectively [see Fig. 2(b)]. The transmittance amplitude decays to half its maximum value in an optical bandwidth of 4.5 nm. Finally, when the acoustic frequency is varied, the periodicity of the perturbation also changes, and

hence the phase-matching condition is shifted to a different wavelength at a measured rate of −0.325 nm/kHz. However, not every acoustic frequency is equally satisfactory for achieving high enough modulation, due to the combination of the nonflat frequency response of the piezoelectric and the acoustic fiber resonator.

The setup of the actively mode-locked fiber ring laser is schematically illustrated in Fig. 3. The medium gain was provided by $L_{\mathrm{EDF}} = 2.5$ m of erbium-doped fiber (EDF) containing 300 ppm Er^{3+}, with a cutoff wavelength of 939 nm and a numerical aperture of 0.24. The active fiber was pumped through a 980/1550 nm wavelength division multiplexer (WDM) coupler by a pigtailed laser diode, providing a maximum pump power of 500 mW at 980 nm. Next—and following a clockwise direction—it was inserted into the AOM preceded by a polarization controller (PC), followed by a delay line fusion-spliced to a 10 dB coupler. Finally, the ring cavity was closed by inserting a polarization-independent optical isolator between the optical coupler and the WDM, in order to force unidirectional operation within the ring. In this way, the entire laser is spliced. The output of this laser is obtained from the 10 dB port of the optical coupler.

In an active mode-locked laser the round-trip time must be matched with the reciprocal of the optical modulation frequency. Since we selected the same operation point shown in Figs. 1 and 2—i.e., $f_m = 1.538$ MHz—and by taking as modal effective index $n = 1.469$, it results in a cavity length $L = c/n \times 1/f_m = 132.69$ m, with c the speed of light in vacuum. The optical fiber component length L_{OFC}, obtained by adding up the lengths of the optical isolator, WDM, AOM, and optical coupler (see Fig. 3), was $L_{\mathrm{OFC}} = 3.95$ m. Therefore, it is necessary to have a delay line length of $L - L_{\mathrm{EDF}} - L_{\mathrm{OFC}} = 126.24$ m. This delay line was made by combining 42.68 m of Fibercore SM980 ($D = -4.09$ ps/nm km) with 83.56 m of Corning LEAF ($D = 2$ ps/nm km), where D is the dispersion of the optical fibers. This, plus taking $D = -18.8$ ps/nm km for the EDF, results in a slightly normal average dispersion of this cavity with a value of −0.154 ps/nm km. It is important to remark that a fine adjustment of the cavity length is always necessary in order to match the reciprocal of the optimal modulation frequency with the cavity round-trip time, especially in a long-cavity fiber laser, where several cuts and splices of different fibers and fiber components are present. For example, a cavity assembled with an error in length $\Delta L/L$ would shift the necessary modulation frequency in the same quantity, i.e., $\Delta f_m/f_m$. However, as we discussed before when we characterized the AOM, this could shift the modulation frequency to a nonsatisfactory operation point (in terms of modulation depth), due to the nonflat frequency response of the tandem piezoelectric plus the acoustic fiber resonator. For this reason, it is important to find some procedure that maximizes the accuracy in the cavity length. We solved this problem by launching a short pulse into the cavity by the free port of the optical coupler (see Fig. 3), and measuring the successive round-trip times τ, with the AOM switched-off plus a moderate pump power to compensate for the attenuation in the EDF. Therefore, once the cavity was assembled, the fiber length ΔL to be removed/added to the cavity could be obtained from $\Delta L = (\tau - 1/f_m) \times c/n$, depending on whether $\Delta L > 0$ or $\Delta L < 0$, respectively. For these long-cavity lasers, the necessary correction is generally in the tens-of-millimeters range. Regarding the AOM, it is worth mentioning that coupling to some other cladding modes was also observed in our experiments; e.g., there is another transmission dip at 1700 nm, when the same flexural acoustic wave at 769 kHz travels down the AOM. However, this coupled light has no consequences in the mode-locking operation, not only because it fulfills the phase-matching condition at optical wavelengths well beyond the maximum of the EDF gain but because of the filtering action of the WDM and other optical components along the laser's cavity.

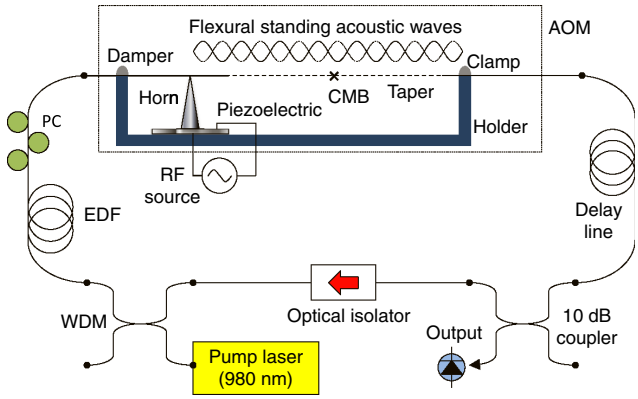

Fig. 3. Setup of the actively mode-locked all-fiber ring laser. The dashed line represents the tapered optical fiber.

The laser's performance was investigated for a wide range of system parameters. Figure 4(a) depicts the laser behavior, showing the train of optical pulses generated at a frequency of 1.538 MHz (emission wavelength $\lambda_0 = 1534.45$ nm), plus the applied voltage to the piezoelectric. Figure 4(b) shows the oscilloscope trace (50 GHz bandwidth), exhibiting a narrow single mode-locked pulse of 330 ps pulse width and 120 mW peak power for a CW pump power of 130 mW, superimposed on a 10 ns width pedestal. The short pulse contains 10% of the full pulse energy, i.e., the pedestal plus short pulse. The pump power threshold was 50 mW, and the pedestal was present at every pump power regime up to the maximum available pump power in our setup (500 mW). Regarding the detuning characteristics of this laser, a 10 Hz mismatch in either direction is enough to lose the narrow mode-locked pulse. However the pedestal still persisted

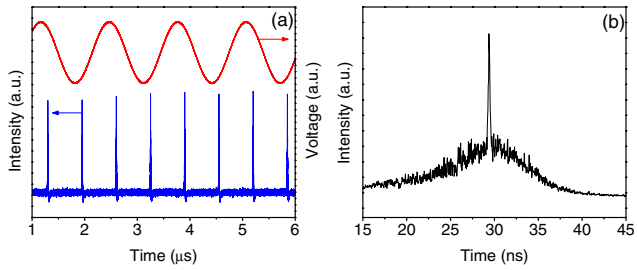

Fig. 4. (a) Mode-locked train of pulses generated at a 1.538 MHz repetition rate with 130 mW of pump power (blue curve, left axis) and modulation voltage of 0.769 MHz and 40 V (red curve, right axis). (b) A single mode-locked pulse with a FWHM of 330 ps.

up to the maximum allowable detuning of 1 kHz. This result proves that only a minor fraction of the AOM's optical bandwidth is exploited to mode lock. In the same line, Fabert *et al.* recently reported unsatisfactory active mode locking in a long-cavity all-fiber laser (220 and 135 m length), with output light pulses as broad as 60 ns in both cases [11]. The impossibility of obtaining short pulses in active mode locking at low repetition rates could be related to the use of sinusoidal amplitude modulation. In that case, the transmission window is also sinusoidal, and therefore, as the cavity is elongated, the repetition rate decreases, and the window becomes increasingly wider, leading to broad pulses. A similar trend is also reported in passive mode locking, when the cavities are elongated up to several hundred meters, with output light pulses well above the nanosecond regime [1–3]. This situation substantially changes if the modulator can be driven by a short pulse. In that case, the transmission window can be kept short enough, independent of a long repetition rate. The results obtained by Schlager *et al.* and Kafka *et al.* are along these lines [12,13]. In the former, output light pulses in the tens of picoseconds regime were obtained for cavities elongated up to 5 km. In both cases this was possible by using an integrated electro-optic intensity modulator driven by a subnanosecond pulse generator. Of course, in that situation, many interesting features of an all-fiber configuration are lost. Alternatively, by using a nonlinear optical loop mirror, it is possible to filter out the broad pedestal at the output [14].

We also varied the EDF length from 1 to 3.5 m in 0.5 m steps, while simultaneously varying the delay line length in order to keep constant the final cavity length of 132.69 m. At 1.5 m of EDF length, mode-locked pulses of 158 ps superimposed on a 10 ns width pedestal were obtained at 126 mW of pump power, whereas at 1 m of EDF length it was not possible to achieve pulsed lasing emission.

Finally, we used different delay lines in order to reverse the sign of the average dispersion of the cavity, i.e., from normal to anomalous. Thus, we tested two different delay lines, first by using Corning LEAF, and then SMF-28 ($D = 16$ ps/nm km), with final average dispersions of 1.42 and 14.74 ps/nm km, respectively. In both cases the behavior was similar to that shown in Fig. 4, exhibiting a narrow single mode-locked pulse of 200 and 580 ps pulse width over a wide pedestal. The peak power P_0 required to support a fundamental soliton pulse within this cavity can be obtained from $P_0 = |\beta_{20}|/\gamma T_0^2$, where β_{20} is the second-order derivative of the propagation constant—related to D by $\beta_{20} = -\lambda_0^2 D/2\pi c - T_0 = 0.2$ ns is the half-width at the $1/e$ intensity point of the pulse, and γ is the nonlinear parameter. In both cases the measured peak power (120 mW) greatly exceeds the power of the fundamental soliton pulse, i.e., $P_0 = 0.03$ and 0.37 mW when Corning LEAF and SMF-28, respectively, were used as delay lines (the nonlinear parameter was approximately the same in both cases, i.e., $\gamma = 0.001$ W^{-1}/m). Thus, our conclusion is that soliton pulse shaping was not observed.

This work has been financially supported by the Ministerio de Educación y Ciencia and the Generalitat Valenciana of Spain (projects TEC2008-05490 and PROMETEO/2009/077, respectively). C. Cuadrado-Laborde acknowledges the Programa de Investigadores Invitados de la Universidad de Valencia (Spain).

References

1. S. Kobtsev, S. Kukarin, and Y. Fedotov, Opt. Express **16**, 21936 (2008).
2. X. Li, X. Liu, X. Hu, L. Wang, H. Lu, Y. Wang, and W. Zhao, Opt. Lett. **35**, 3249 (2010).
3. V. I. Denisov, B. N. Nyushkov, and V. S. Pivtsov, Quantum Electron. **40**, 25 (2010).
4. H. Sayinc, D. Mortag, D. Wandt, J. Neumann, and D. Kracht, Opt. Express **17**, 5731 (2009).
5. C. Cuadrado-Laborde, A. Díez, M. V. Andrés, J. L. Cruz, M. Bello-Jimenez, I. L. Villegas, A. Martínez-Gámez, and Y. O. Barmenkov, in *Acoustic Waves from Microdevices to Helioseismology*, M. G. Beghi, ed. (InTech, 2011), pp. 595–636.
6. M. Bello-Jiménez, C. Cuadrado-Laborde, D. Sáez-Rodríguez, A. Diez, J. L. Cruz, and M. V. Andrés, Opt. Lett. **35**, 3781 (2010).
7. C. Cuadrado-Laborde, A. Díez, J. L. Cruz, and M. V. Andrés, Laser Photon. Rev. **5**, 404 (2011).
8. H. S. Kim, S. H. Yun, I. K. Kwang, and B. Y. Kim, Opt. Lett. **22**, 1476 (1997).
9. K. Lee, D. Yeom, and B. Kim, Opt. Express **15**, 2987 (2007).
10. Y. G. Han, S. H. Kim, S. B. Lee, U. C. Paek, and Y. Chung, Electron. Lett. **39**, 1107 (2003).
11. M. Fabert, V. Kermene, A. Desfarges-Berthelemot, P. Blondy, and A. Crunteanu, Opt. Lett. **36**, 2191 (2011).
12. J. B. Schlager, Y. Yamabayashi, D. L. Franzen, and R. I. Juneau, IEEE Photon. Technol. Lett. **1**, 264 (1989).
13. J. Kafka, D. Hall, and T. Baer, Opt. Lett. **14**, 1269 (1989).
14. M. Bello-Jiménez, E. Kuzin, O. Pottiez, B. Ibarra-Escamilla, A. Flores-Rosas, and M. Durán-Sánchez, Opt. Express **18**, 2090 (2010).